P1.3

Wave propagation and PV-pulses from diurnal mountain convection

Yanping Li and Ronald B. Smith,
Yale University, Connecticut, USA

1. INTRODUCTION

The diurnal cycle of summer convection over mountains is thought to generate disturbances that can modulate convection nearby (Banta and Schaaf, 1987), and possible at a great distance. An example is the propagation of convection from the Rockies eastward, even reaching the Atlantic coast (Carbone et al.2003). A basic question is whether diurnal gravity waves play a role in such events? If they do, how are they modified by rotation, mean wind and shear? Rotation allows convective heating to generate Potential Vorticity (PV). Daily pulses of PV will drift downwind of the source region, but can they generate vertical motion to trigger convection? Here, we review idealized models based on the classical 3-D linearized Boussinesq equations to see if they can provide new and useful insights.

2. MODELS

Classical 3-D linearized Boussinesq equations are used to demonstrate the effect of periodic heating and rotation. The transient linear response of the atmosphere to prescribed heat sources and sinks has been investigated by Lin and Smith (1986). They discussed the two dimensional, inviscid, nonrotating and hydrostatic flow under different heat forcing. Here, based on these, we add damping, rotation and nonhydrostatic effects under periodic heating force.

The governing equations are:

$$\frac{D\vec{V}}{Dt} + f\vec{k}\times\vec{V} = -\nabla p' - \alpha\vec{V}$$

$$\frac{Db}{Dt} - N^2 w = B - \alpha b$$

$$\nabla\cdot\vec{V} = 0$$

Here, $p' = (p - \bar{p}(z))/\rho$

Buoyancy: $b = g(T - T_0 + gz/C_p)/T_0$

For periodic heating: $B = g\dot{Q}/\rho_0 C_p T_0$

We assume the scaled heating rate:

$B(x,y,z,t) = B_\sigma(x,y,z)e^{i\sigma t}$

σ is the heating frequency. Here, we are not only interested in diurnal but also semi-diurnal heating, since they can be composed to approximate arbitrary oscillating heating.

Use the Gauss function as horizontal heating function:

$B_\sigma(x,y,z) = Ae^{-(ax^2+by^2)}f(z)$

3 SINGLE LAYER MODEL RESULTS

1-layer linear model is able to illustrate the condition for the generation of inertio-gravity waves (IGW). Here, we'll emphasize on the relation between σ, U, and f.

We use two dimensional Fourier transform in x,y and simplify original equations to

$$\hat{w}_{zz} + \gamma^2\hat{w} = \frac{\hat{B}(k^2+l^2)}{\bar{\sigma}^2 - f^2}f(z)$$

Here, $\gamma^2 = \frac{N^2(k^2+l^2)}{\bar{\sigma}^2 - f^2}$ for hydrostatic flow. And intrinsic frequency $\bar{\sigma} = \sigma + Uk + Vl - i\alpha$, which is also the dispersion relation. It reflects the Doppler shift of the heating frequency by the mean wind.

The characteristic vertical wavenumber γ determines the solution character of $\hat{w}(z)$. If $\gamma^2 > 0$, the vertical motion will be periodic in z direction. If $\gamma^2 < 0$, the perturbation will damp with z, no wave will be generated. So the condition for the generation of IGW is $\bar{\sigma}^2 - f^2 > 0$.

The solution of PV in Fourier Space is

$$\hat{PV} = \varsigma + \frac{f}{N^2}b_z = \frac{f}{N^2}\frac{\hat{B}}{i\bar{\sigma}}f'(z)$$

So, if $f = 0$ or $\hat{B} = 0$ or $f'(z) = 0$, $\hat{PV} = 0$, which means that PV couldn't exist without Coriolis force, or outside heating region, or constant heating magnitude in z direction.

Here, we demonstrate three numerical FFT (Fast Fourier Transform) results:

The parameters that the 1-layer linear models used are: inner domain 400 grid cell × 10km; outer domain 16384 grid cell × 10km; mean wind U; Rayleigh Decay constant α; Coriolis parameter f; depth of heating H=2000m, $\beta = 1/H$; horizontal Gauss shape of heating, the radius of the source a grid cell × 10km; the heating strength 2.5×10^{-6}.

Case	f (s^{-1})	U (m/s)	$\bar{\sigma}$ (s^{-1})	$\bar{\sigma}^2 - f^2$	Motion
1A	0	0	σ_D	>0	GW, no PV
1B	10^{-4}	0	σ_D	<0	Local disturbance, PV generated
1C	10^{-4}	10	$\sigma_D + Uk$	>0 ($k>0$)	Upwind: IGW, No PV
				<0 ($k<0$)	Downwind: Local disturbance, PV advected downwind

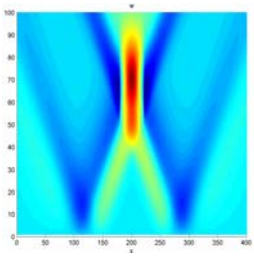

Fig 1.1

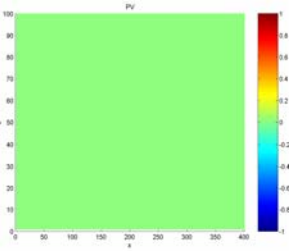

Fig 1.2

Case 1A simulates a diurnal oscillating, non-advective, nonrotating flow. Fig 1.1 shows w field of case 1A. Fig 1.2 shows PV field of case 1A. The horizontal axis is x (10km per grid). The vertical axis is z (100m per grid). Since the oscillating heating effect is dominant $(\sigma > f)$, it generates gravity waves. These gravity waves propagate to both sides, and are reflected from the rigid lower boundary. No PV is generated because of no Coriolis force.

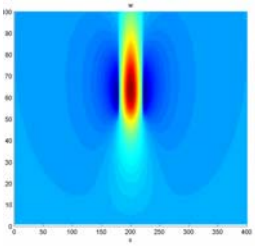

Fig 2.1

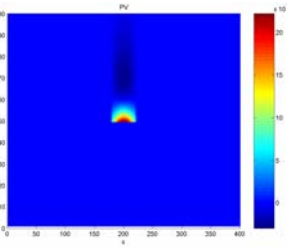

Fig 2.2

Case 1B simulates a diurnal oscillating, non-advective, rotating flow. Fig 2.1 shows w field. Fig 2.2 shows PV field. Since the Coriolis force effect is dominant $(\sigma < f)$, the disturbance will decay with height. Waves are cut off, only local disturbances exist. PV is generated but only in the heating area.

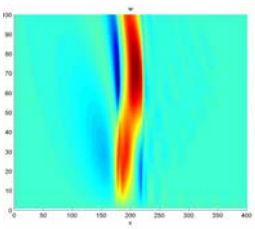

Fig 3.1

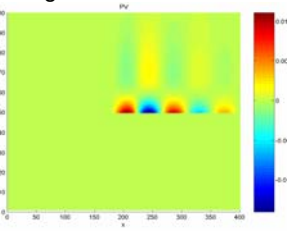

Fig 3.2

Case 1C simulates a diurnal oscillating, strongly advective, rotating flow. Fig 3.1 shows w field. Fig 3.2 shows PV field. Since the effects of oscillation and rotation are comparable, the advection becomes important. In the upwind side, inertio-gravity waves are generated; in the downwind side, they are cut off. PV are generated at the heating source and advected downwind. No vertical motion is associated with the advected PV pulse.

4. 2-LAYER MODEL RESULTS

4.1 Parameters in the model

2-layer linear model is based on the 1-layer model, but vertical shears of U_1/U_2 and N_1/N_2 are added. This model is capable of illustrating the vertical wind shear, stability changing with height in troposphere.

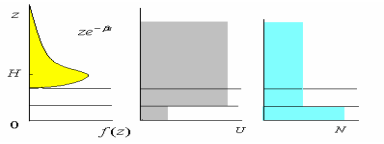

4.2 General analytic solutions

In order to demonstrate the effect of the vertical shear, first, we solve 2-layer Linearized Boussinesq equations in Fourier space:

$I.\ 0 \le z < z_1$

$$\hat{w}_1(z) = \frac{\bar{\sigma}_1}{\bar{\sigma}_2} \cdot \frac{-ie^{i\gamma_1 z_1 - i\gamma_2 z_1}}{(\bar{\sigma}_1^2 - f^2)\gamma_1(e^{2i\gamma_1 z_1}+1) - (\bar{\sigma}_2^2 - f^2)\gamma_2(e^{2i\gamma_1 z_1}-1)} \frac{\hat{B}(k^2+l^2)}{(i\gamma_2-\beta)^2}(e^{i\gamma_1 z} - e^{-i\gamma_1 z})$$

$II.\ z_1 \le z < H$

$$\hat{w}_2(z) = \frac{\gamma_1}{i\gamma_2} \frac{e^{2i\gamma_1 z_1}+1}{(\bar{\sigma}_1^2 - f^2)\gamma_1(e^{2i\gamma_1 z_1}+1) - (\bar{\sigma}_2^2 - f^2)\gamma_2(e^{2i\gamma_1 z_1}-1)} \cdot \frac{\hat{B}(k^2+l^2)}{(i\gamma_2-\beta)^2} e^{i\gamma_2 H - 2i\gamma_2 z_1} e^{i\gamma_2 z}$$

$$+ \frac{\hat{B}(k^2+l^2)}{(\bar{\sigma}_1^2 - f^2)2i\gamma_2} \frac{1}{(i\gamma_2-\beta)^2}\left[e^{i\gamma_2 H - 2i\gamma_2 z_1} e^{i\gamma_2 z} + e^{i\gamma_2 H} e^{-i\gamma_2 z}\right]$$

$III.\ z \ge H$

$$\hat{w}_3(z) = \frac{\gamma_1}{i\gamma_2} \frac{1+e^{-2i\gamma_2 z_1}}{(\bar{\sigma}_1^2 - f^2)\gamma_1(e^{2i\gamma_1 z_1}+1) - (\bar{\sigma}_2^2 - f^2)\gamma_2(e^{2i\gamma_1 z_1}-1)} \cdot \frac{\hat{B}(k^2+l^2)}{(i\gamma_2-\beta)^2} e^{i\gamma_2 H} e^{i\gamma_2 z}$$

$$+ (e^{-2i\gamma_2 z_1} + e^{-2i\gamma_2 H}) \frac{\hat{B}(k^2+l^2)}{(\bar{\sigma}_1^2 - f^2)2i\gamma_2} \frac{1}{(i\gamma_2-\beta)^2} e^{i\gamma_2 H} e^{i\gamma_2 z}$$

And $\hat{PV}_n = \frac{f}{N^2} \frac{\hat{B}(k,l) f'(z)}{i\bar{\sigma}_n} \quad n = 1,2,3$

4.3 Asymptotic integral evaluation to get the far field solution

To simplify the discussion, we set $l = 0$ here.

In real space,

$$w_n(x,z,t) = e^{i\sigma t}\int \hat{w}_n(k,z)e^{ikx}dk\ ,\ PV_n(x,z,t) = e^{i\sigma t}\int \hat{PV}_n(k,z)e^{ikx}dk$$

If the solution of $\hat{w}_n$ exist, the eigenvalue γ_n should be finite, which means $\bar{\sigma}_n^2 - f^2 \ne 0$. Also, the definition of γ_n make sure γ_n is finite and $\gamma_n \ne 0$, otherwise $k^2 + l^2 = 0$, which is impossible. The imaginary part of $\gamma_n \ge 0$ make sure $(i\gamma_n - \beta) < 0$. So the possible poles for the integral are $\bar{\sigma}_2 = 0$ and $(\bar{\sigma}_1^2 - f^2)\gamma_1(e^{2i\gamma_1 z_1}+1) - (\bar{\sigma}_2^2 - f^2)\gamma_2(e^{2i\gamma_1 z_1}-1) = 0$.

The latter one equals to

$$\tan(\gamma_1 z_1) = -i \cdot \frac{\bar{\sigma}_1^2 - f^2}{\bar{\sigma}_2^2 - f^2} \cdot \frac{\gamma_1}{\gamma_2}$$

Which is resonance condition. But the choose of physical parameters here (a, U_1/U_2, N_1/N_2, σ, f) is impossible to satisfy this resonance condition. So, there will not exist singularity for $\hat{w}_2(k,z)$ and $\hat{w}_3(k,z)$, since $\gamma_2 \ne 0$, $(i\gamma_2 - \beta) \ne 0$. But it is possible for $\bar{\sigma}_n = 0$.

When $\bar{\sigma}_2 = 0$, $\sigma + U_2 k^* = 0$, $k^* = -\frac{\sigma}{U_2}$, it will become a singularity to $\hat{w}_1(k,z)$ and $\hat{PV}_3(k,z)$.

Since γ_n, $\frac{k^2}{\bar{\sigma}_2^2 - f^2}$ are all rational function of k, and the degree of numerator and denominator are the same, which means that when k goes to infinity, they goes to some specific values. So, $\hat{w}_3(k,z) = f(k^0)e^{ik^0 z}\hat{B}$, and $\left|f(k^0)e^{ik^0 z}\right| < M$ when $k \to \infty$. But $\hat{B} = Be^{-\frac{k^2}{a^2}}$, when $k \to \infty$, $\hat{B} \to 0$. So $\int \left|\hat{w}_3(k,z)\right| dk < \infty$. According to Riemann-Lebesgue Lemma, $\int \hat{w}_3(k,z)e^{ikx}dk \to 0$ when $x \to \infty$. $\hat{w}_2(k,z)$ is also the same.

But $\hat{w}_1(k,z)$ has singularity for $k^* = -\frac{\sigma}{U_2}$. And

$$\int_{-\infty}^{\infty} \hat{w}_1(k,z)e^{ikx}dk = \int_{-\infty}^{\infty} f(k)\frac{1}{\sigma + U_2 k}\left[e^{i\gamma_1(k)z} - e^{-i\gamma_1(k)z}\right]e^{ikx}dk .$$

This integral can be easily evaluated by using contour integration.

$$w_1(x,z,t) = 2\pi i \,\mathrm{Re}\, s(k^*)e^{i\sigma t}$$

$$= -4\pi f(k^*)Sin\left[\gamma_1(k^*)z\right]e^{-i\frac{\sigma}{U_2}(x-U_2 t)}e^{-\frac{\alpha_2}{U_2}x}$$

Also

$$PV_3(x,z,t) = 2\pi i \,\mathrm{Re}\, s(k^*)e^{i\sigma t}$$

$$= 2\pi \frac{f}{N_2^2}\cdot f'(z)e^{-i\frac{\sigma}{U_2}(x-U_2 t)}e^{-\frac{\alpha_2}{U_2}x}$$

Which means that $w_1(x,z,t)$ and $PV_3(x,z,t)$ propagate downwind with the same speed U_2. And the term $Sin\left[\gamma_1(k^*)z\right]$ determines the vertical structure of w_1. If $\gamma_1(k^*)$ is real, $w_1(x,z,t)$ is periodic in z direction, which corresponds to gravity waves in the lower layer ($\gamma_1^2 > 0$). If $\gamma_1(k^*)$ is imaginary, $w_1(x,z,t)$ decays with height ($\gamma_1^2 < 0$), which corresponds to quasi-geostrophic (QG) motion.

By the way, the singularity of $\hat{w}_1(k,z)$ caused only when $\bar{\sigma}_1 \neq \bar{\sigma}_2$. If $\bar{\sigma}_1 = \bar{\sigma}_2$, no matter $\bar{\sigma}_2 = 0$, the nominator $\bar{\sigma}_1$ cancels with the denominator $\bar{\sigma}_2$, no singularity causes. This means that if no shears exist, $w_1(x,z,t) \to 0$ when $x \to \infty$, no matter PV drifting with mean wind or not. This result is consistent with the general conclusion that vertical motion is invariant under a Galilean transformation of the zonal coordinate.

4.4 Numerical FFT results for 2-layer linear model

Here, we demonstrate two numerical FFT results for the 2-layer model:

Case	σ s^{-1}	f s^{-1}	U_1/U_2 m/s	Motion	
2A	σ_D	10^{-4}	1/10	Upwind	II: IGW
					I: QG
				Downwind	II: PV, IGW
					I:QG
2B	$2\sigma_D$	10^{-4}	1/10	Upwind	II: IGW
					I: IGW
				Downwind	II: PV, IGW
					I: IGW

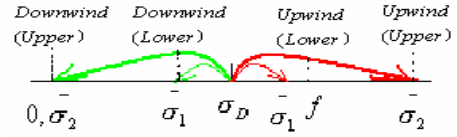

Fig 4.1

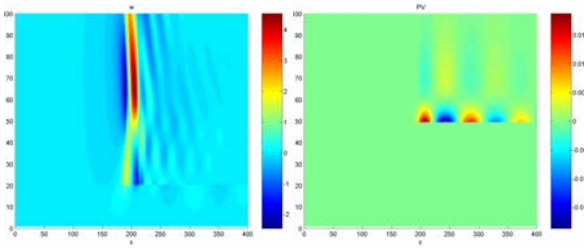

Fig 4.2 Fig 4.3

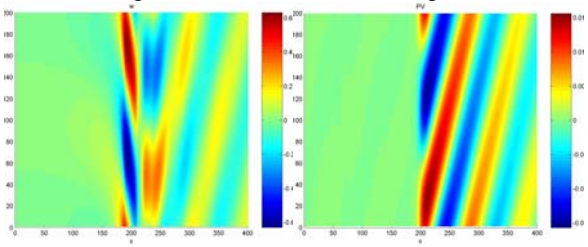

Fig 4.4 Fig 4.5

Case 2A simulates the case with diurnal heating and strong vertical shears. Fig 4.1 is the frequency diagram, it shows that gravity waves generate in the upwind side both in the upper layer and in the lower layer; but in the downwind side, the intrinsic frequency of the lower layer falls into the quasi-geostrophic (QG) region, so only QG perturbation is generated there. Fig 4.2 is the w field. Fig 4.3 is the PV field. The horizontal axis is x (10km per grid). The vertical axis is z (100m per grid). Although near the heating source, there exist local forced circulation. But far away from the source, only the QG perturbation triggered by the drifting PV is dominant. Fig 4.4 is the time-distance plot of the w when z=1800m. Fig 4.5 is the time-distance plot of the PV when z=5200m. The horizontal axis is x (10km per grid). The vertical axis is t (432 second per grid). It can be seen that the propagating QG perturbation in the lower layer and drifting PV in the upper layer have the same speed, which is equal to that of the upper layer mean wind.

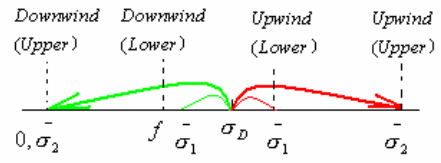

Fig 5.1

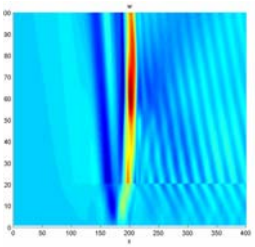

Fig 5.2

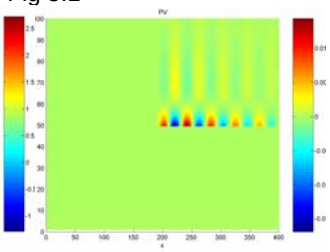

Fig 5.3

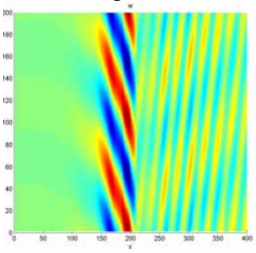

Fig 5.4

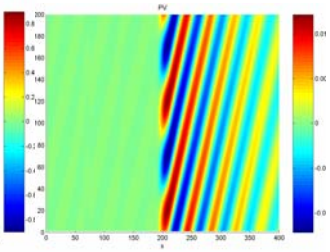

Fig 5.5

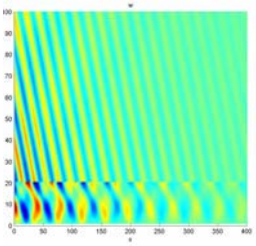

Fig 5.6

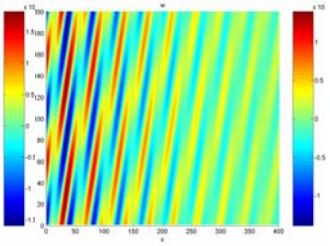

Fig 5.7

Case 2B shows the case with semi-diurnal heating and strong vertical shears. Fig 5.1 is the frequency diagram, it shows that gravity waves (GW) generate in the upwind side both in the upper layer and in the lower layer. And in the downwind side, the intrinsic frequency of the lower layer also falls into the GW region, so GW perturbation is generated there. Fig 5.2 is the w field near the heating source. Fig 5.3 is the PV field near the heating source. Fig 5.4 is the time-distance plot of the w (near the heating source) when z=1800m. Fig 5.5 is the time-distance plot of the PV (near the heating source) when z=5200m. Fig 5.6 is the w field far away from the heating source. Fig 5.7 is the time-distance plot of the w (far away from the heating source) when z=1800m. Near the heating source, there exist gravity waves both in the upwind side and in the downwind side of the upper layer, and in the upwind side of the lower layer, but they decay very fast. So far away from the source, only the GW perturbation triggered by the drifting PV can exist. Here, the local GW near the heating source is different from the GW perturbation triggered by the drifting PV since the former one has different wavelength as that of the PV and their propagation speeds are independent (Fig 5.2, 5.4, 5.7), but the latter one has the same wavelength as that of the PV and they propagate with the same speed (Fig 5.5, 5.7).

5. SUMMARY AND CONCLUSION:

In this paper, general analytical solutions of linearized Boussinesq equations are solved for 1-layer and 2-layer models. 1-layer model results show that the relative magnitude of the intrinsic frequency and Coriolis frequency is important. If $\sigma > f$, inertia gravity waves will be generated; if the Coriolis effect is dominant ($\sigma < f$), waves will be prevented. In mid-latitudes, the diurnal frequency is less than the Coriolis parameter, so gravity wave propagation is prevented. A mean wind Doppler shifts the frequency in principle, but in practice, little gravity wave energy is found either upwind or downwind of the source.

The definition of potential vorticity shows that the generation of PV depends on the existence of the Coriolis force, and a heating source that varies in altitude. Without the Coriolis force, no potential vorticity will be generated.

While the combined role of PV and background shear are already well known in the Q-G limit (e.g. the omega-equation and Q-vectors) we take a linearized gravity wave approach. Within a linear framework, we examine the analytical solution by asymptotic integral evaluation and the numerical FFT results of the linear model. It seems that vertical mean wind shear plays a critical role: a PV pulse drifting in a constant wind, just like a stationary one, will produce no vertical motion according to the principle of Galilean Invariance. In contrast, in a sheared mean wind, the vertical motions will accompany the PV pulse.

In future, we'll see if PV induced vertical motion is strong enough to trigger deep convection through satellite observation and numerical modeling.

6. ACKNOWLEDGEMENTS:

The research is supported by the National Science Foundation, Division of Atmospheric Sciences (ATM-0112354).

References

Banta, R.M. and C.L.B.Schaaf, 1987: Thunderstorm genesis zones in the Colorado Rocky Mountains as determined by traceback of geosynchronous satellite images. *Mon. Wea. Rev.*, **115**, 463-476.

Carbone R.E., J. D. Tuttle, D. A. Ahijvych and S. B. Trier, 2002: Inferences of predictability associated with warm season precipitation episodes. *J. Atmos. Sci.*, 59, 2033-2056.

Smith R. B., 1979: The influence of the earth's rotation on mountain wave drag. *J. Atmos. Sci.*, **36**, 177-180.

Lin, Y.-L., R. B. Smith, 1986: The transient dynamics of airflow near a local heat source. *J. Atmos. Sci.*,**43**, 40-49.